Cooling of radiative quantum-dot excitons by terahertz radiation: A spin-resolved Monte Carlo carrier dynamics model

Fredrik Boxberg,[1,*] Jukka Tulkki,[1] Go Yusa,[2] and Hiroyuki Sakaki[2]
[1]*Laboratory of Computational Engineering, Helsinki University of Technology, P.O. Box 9203, FIN-02015 HUT, Finland*
[2]*Institute of Industrial Science, The University of Tokyo, 4-6-1 Komaba, Meguro-Ku, Tokyo 153-8505, Japan*
(Received 27 December 2006; published 30 March 2007)

We have developed a theoretical model to analyze the anomalous cooling of radiative quantum dot (QD) excitons by THz radiation reported by G. Yusa, *et al.*, [Proceedings of the 24th ICPS, *Teraherz-near infrared upconversion in strain-induced quantum dots*, (World Scientific, Singapore, 1999)]. We have made three-dimensional (3D) modeling of the strain and the piezoelectric field and calculated the 3D density of states of strain induced quantum dots. On the basis of this analysis we have developed a spin dependent Monte Carlo model, which describes the carrier dynamics in QDs when the intraband relaxation is modulated by THz radiation. We show that THz radiation causes resonance transfer of holes from dark to radiative states in strain-induced QDs. The transition includes a spatial transfer of holes from the piezoelectric potential mimima to the deformation potential minimum. This phenomenon strongly enhances the QD ground state luminescence at the expense of the luminescence from higher states. Our model also reproduces the delayed flash of QD ground state luminescence, activated by THz radiation even ~1 s after the carrier generation. Our simulations suggest a more general possibility to cool the radiative exciton subsystem in optoelectronic devices.

DOI: 10.1103/PhysRevB.75.115334 PACS number(s): 73.21.La, 73.23.−b, 78.67.Hc

I. INTRODUCTION

Semiconductor quantum dots (QDs) are commonly called artificial atoms, due to their man-made single-atom-like spectrum, consisting of well separated spectral lines.[1–3] Nevertheless, time-resolved spectroscopy of intraband relaxation sequences has proved to be much more difficult with QDs than with free atoms. It is, in distinction to free atoms, not possible to observe QD intraband relaxation as sequences of well resolved intermediate steps, because the intermediate states are very close in energy and involve many simultaneously excited electrons.

Recently Yusa *et al.* used visible light and near infrared (NIR) radiation in combination with terahertz radiation to study intraband carrier relaxation in strain-induced quantum dots (SIQDs).[4] The experiment of Yusa *et al.*, analyzed theoretically in this work, has remained to our knowledge the only measurement in which the details of the QD intraband relaxation processes have been successfully studied by modulating the dynamics of the carriers, with a radiation field, which is in approximative resonance with the intraband transitions. This has prompted us to make a careful analysis of this experiment in order to emphasize the potential of this experimental approach and to support a detailed planning of further experiments of this kind.

In this work we analyze the experiments of Yusa *et al.* using a spin-resolved Monte Carlo (MC) carrier dynamics model, which is based on new full three-dimensional (3D) strain and electronic structure calculations and furthermore on information extracted from previous time-resolved[5,6] and continuous wave (CW)[7] luminescence measurements, including their computational analysis. We show that deep minima of the piezoelectric potential (PEP) play a key role in the observed anomalous THz-radiation enhancement of the ground state luminescence.

The electronic structure was calculated using continuum elasticity and the multiband $\mathbf{k}\cdot\mathbf{p}$ method, which are well suited for the modeling of relatively large SIQDs (the ground state wave functions have an effective diameter of approximately 15–20 nm).[8] We have made a detailed comparison of the theoretical CW luminescence with experiments and previous axially symmetric calculations. On the basis of this comparison we build a simplified electron and hole structure. This was necessary to make the MC dynamics simulations computationally feasible.

Our semiempirical carrier dynamics model is based on an intuitive description of the key physical processes governing the carrier dynamics of a SIQD. The separate relaxation processes and their governing rate parameters are taken from several previous experiments and from computational analyses of these experiments.[5,6] Our MC model is a generalization of previous master equation models.[5,6,9] It includes the spin of the carriers and by accounts for the piezoelectric potential minima.

We emphasize that fully *ab initio* calculations of the studied electron-hole system, including, for instance, correlation effects in a nonperturbative way, is at present not computationally feasible. However, we hope that our work will prompt for detailed studies of correlation effects as well as for advanced studies of the electronic structure using microscopic theories.[10]

II. ELECTROELASTICITY AND BAND STRUCTURE

The understanding of SIQDs has until now relied on a simplified axisymmetric description of the electronic structure.[11] In this work we have carried out extensive three-dimensional modeling of the electroelastic, electronic, and photonic properties of SIQDs. We emphasize the role of the PEP, not present in previous two-dimensional models of the carrier dynamics. Figure 1(b) shows our SIQD model geometry, which is based on transmission electron micrographs of SIQDs.[12]

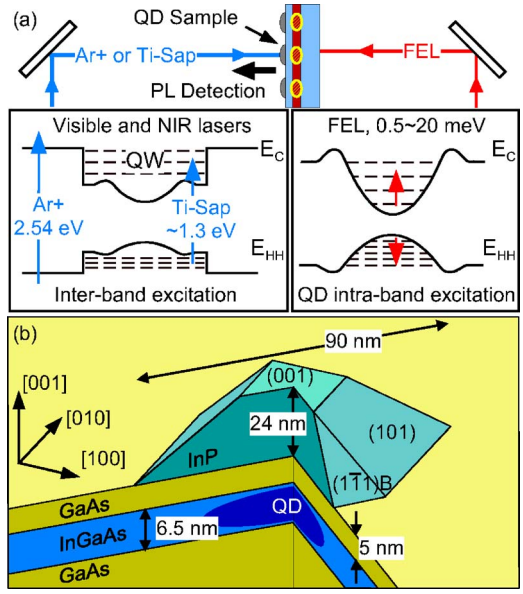

FIG. 1. (Color online) (a) In the analyzed experiment (Ref. 4), the QD sample was pumped by either an Ar+ or Ti-Sap laser. The QD intraband dynamics was modulated by a free electron laser (FEL). (b) Strain-induced quantum dot in an $In_{0.2}Ga_{0.8}As$ QW, strained by an InP island. The island is defined by the crystal planes {001}, {101}, and {111}.

A. Atomic structure

The elastic strain and the related piezoelectric potential were calculated using the finite element method within the continuum elasticity (CE) approximation. This was motivated by the large geometry, spanning over $\sim 10^8$ atoms and the possibility to include piezoelectric coupling in the model. In the coupled electroelastic field formulas, the vectors of the stress **T** and the electric flux **D** are related to the strain **S** and the electric field **E** as[13]

$$\begin{bmatrix} \mathbf{T} \\ \mathbf{D} \end{bmatrix} = \begin{bmatrix} \mathbf{C} & \mathbf{e} \\ \mathbf{e}^T & -\boldsymbol{\varepsilon} \end{bmatrix} \begin{bmatrix} \mathbf{S} \\ -\mathbf{E} \end{bmatrix}. \quad (1)$$

The symmetry of the crystal enters Eq. (1) through the elasticity matrix **C** and the piezoelectric matrix **e**. The dielectric properties of the materials are described by the dielectric matrix $\boldsymbol{\varepsilon}=\varepsilon \mathbb{1}_{3\times 3}$.

The lattice mismatch was introduced into Eq. (1) by expanding the different materials isotropically according to their lattice mismatch with respect to the GaAs substrate $\Delta a_j=(a_j-a_{\mathrm{GaAs}})/a_j$, where a_j is the lattice constants of either InP or InGaAs and a_{GaAs} is the lattice constant of GaAs. Equation (1) was solved iteratively,[14] using tetrahedral second order elements and the CE parameters given in Table I.

Figure 2 shows the computed strain-induced electron and hole potentials in the middle of the quantum well (QW).[15] The total potential is the sum of the band-edge discontinuity, deformation, and piezoelectric potentials. The elastic strain gives rise to the main deformation potential (DP) minima in the center. The PEP gives, on the contrary, rise to large side minima and side barriers of holes, located near the edges of the InP island. The effect of the PEP on the center minima is, however, small.

TABLE I. Material parameters from Landolt-Börnstein (Ref. 27) unless otherwise noted.

Parameter	GaAs	$In_{0.1}Ga_{0.9}As$	InP
a_0 (Å)	5.65	5.69	5.87
c_{11} (10^{11} dyn cm^{-2})	11.90	11.50	10.11
c_{12} (10^{11} dyn cm^{-2})	5.38	5.29	5.61
c_{44} (10^{11} dyn cm^{-2})	5.95	5.75	4.56
e_{14} (C m^{-2})	−0.16	−0.15	−0.04(Ref. 28)
ε_r	12.53	12.70	13.90

B. Electronic structure

The electronic structure of the QDs was calculated using the eight-band $\mathbf{k}\cdot\mathbf{p}$ method,[16–18] accounting for band edge discontinuity, strain-induced deformation potentials, and the piezoelectric potential. The eight-band $\mathbf{k}\cdot\mathbf{p}$ Hamiltonian can be divided in a strain-free part and a strain part. The strain-free part is parametrized by the band gap E_g, the spin-orbit splitting energy Δ, the optical matrix element E_p, the valence band offset (VBO), the modified Luttinger parameters γ_1, γ_2, and γ_3, the conduction band effective mass m_e, and Kane's parameter B. The strain part, on the other hand, is parametrized by the deformation potentials a_c, a_v, b_v, and d_v. Moreover, it contains the six components of the symmetrized strain tensor ε_{xx}, ε_{yy}, ε_{zz}, ε_{xy}, ε_{yz}, ε_{xz}, and the piezoelectric potential ϕ_{piez}.[12]

The eight-band $\mathbf{k}\cdot\mathbf{p}$ Hamiltonian was discretized using the finite difference technique and diagonalized using the implicitly restarted Lanczos method.[19] For more details on the electronic structure calculations see Ref. 13. The material parameters used in the eight-band $\mathbf{k}\cdot\mathbf{p}$ calculations are listed in Table II. The value of the conduction-valence band coupling parameter E_p, given in Table II, has been reduced in

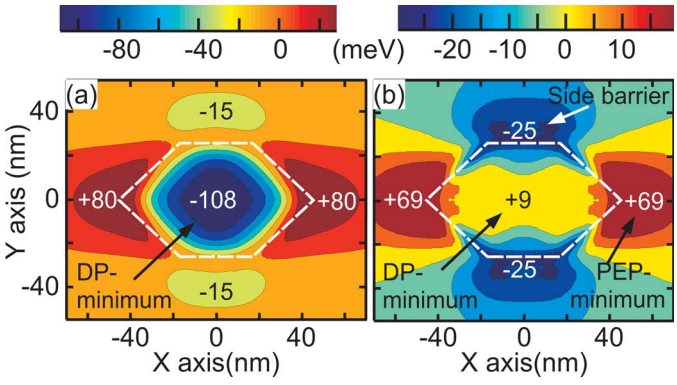

FIG. 2. (Color online) Potential energy of (a) electrons and (b) holes, in the middle of the QW (8.25 nm below the InP island). The energies are given with respect to the band edges of an $In_{0.2}Ga_{0.8}As$ QW, far away from the island. The white dashed lines show the bottom contour of the InP island and the labels correspond to the local potential maxima/minima.

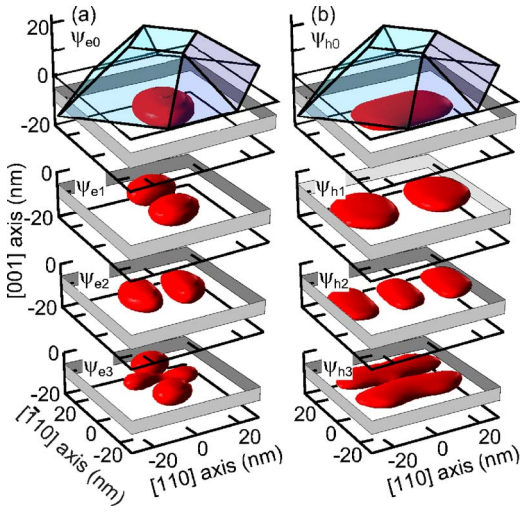

FIG. 3. (Color online) (a) Electron and (b) hole probability densities of the four eigenstates, lowest in energy. The position of the QW is shown by the gray faces.

order to avoid spurious states (see Ref. 13, and references therein). However, the effect of the reduction of E_p on the effective masses was negligible (this was verified by testing the model for the pertinent bulk semiconductors).

The depth of the PEP minima (+69 meV, see Fig. 2) of holes exceeds that of the DP minimum (+9 meV) by tens of meV. The PEP minima have consequently many confined hole states and it is, therefore, energetically more favorable for the holes to populate the deepest PEP states before occupying the DP states. The electrons are, however, mainly confined in the DP minimum (−108 meV), which over-rules the shallow PEP minima of electrons (−15 meV). Spatially separated electron (located on the DP ground state e_1) and hole (on the PEP level p_1) pairs have several decades smaller probability of recombining radiatively than an exciton confined to the DP levels e_1 and h_1.

Figure 3 shows the probability densities of the lowest optically active electron and hole states, confined in the DP minima in the center of the SIQD. Figure 4 shows the density of states (DOS) of all (bright and dark) confined states, including also the hole states confined in the PEP minima (dark). The eigenenergies of Fig. 4 are given with respect to the strain-free band edge energy of the QW material.

TABLE II. Eight-band $\mathbf{k}\cdot\mathbf{p}$ parameters from Ref. 29.

Parameter	GaAs	$In_{0.1}Ga_{0.9}As$
E_g (eV)	1.519	1.366
Δ (eV)	0.341	0.332
γ_1	2.556	3.464
γ_2	−0.152	0.295
γ_3	0.718	1.148
m_e	0.067	0.062
E_p[a] (eV)	20.160	19.742
VBO (eV)	−0.055	0.000
a_v (eV)	1.160	1.144
a_c (eV)	−7.170	−7.196
b_v (eV)	−2.000	−1.980
d_v (eV)	−4.800	−4.680
ε_r[b]	12.530	12.727

[a]These are the used value of E_p and are slightly smaller than the values given in Ref. 29. This was as explained in the text.
[b]Ref. 27.

C. Photoluminescence

The PL intensity was calculated by summing over the transition rates from all electron states to all hole states. The differential photoluminescence rate (rate of spontaneous emission of photons) of light with the polarization $\boldsymbol{\alpha}$ is given by

$$I_{\boldsymbol{\alpha}}(E) \propto \sum_{i,f} \frac{g(E)}{E} |\langle \Psi_{ei}| \boldsymbol{\alpha}^* \cdot \mathbf{p} |\Psi_{hf}\rangle|^2 f_e(E_i) f_h(E_f) P\{[E - (E_i - E_f)], \Gamma\}, \quad (2)$$

where $g(E)$ is the density of photon states [$g(E) \propto E^2$ for a 3D system, i.e., in the absence of a cavity], E_i and E_f are the eigenenergies of the initial electron states $|\Psi_{ei}\rangle$ and the final hole states $|\Psi_{hf}\rangle$. The inhomogeneous linewidth broadening

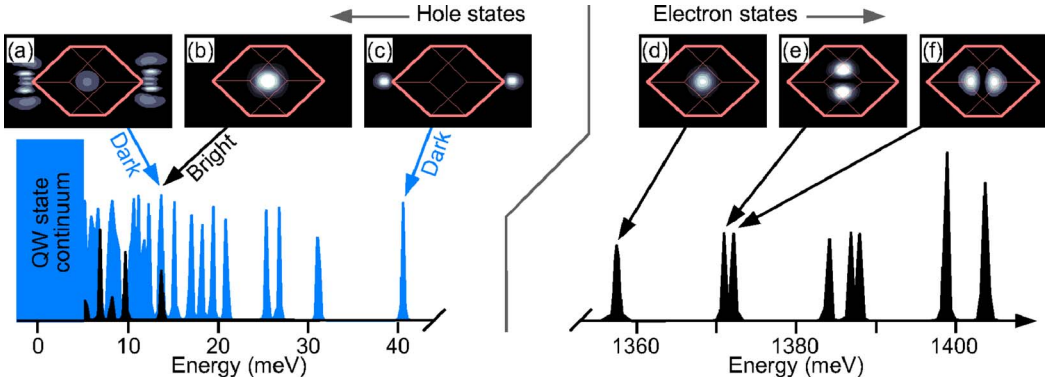

FIG. 4. (Color online) Density of hole and electron states, including states confined in the DP and PEP minima. The blue/gray curve is the total DOS while the black curve corresponds to the DOS of carriers confined in the DP minima only, i.e., the optically active states. The top panels (a)–(f) show the probability densities of selected states, with respect to the position of the InP island (red lines) above the QD.

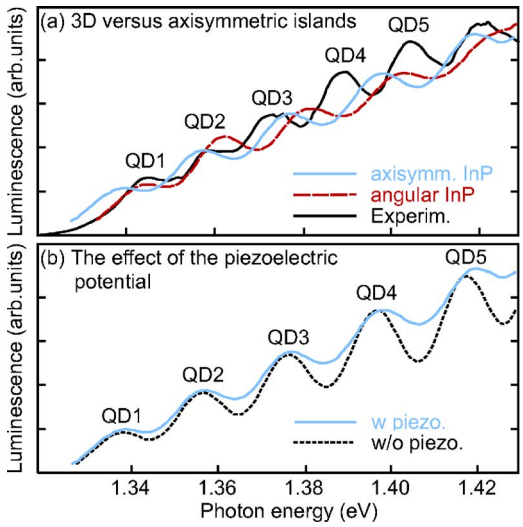

FIG. 5. (Color online) Simulated CW PL (gray/colored lines) in comparison with experimental (Ref. 7) data (black solid line). Figure 5(a) shows the effect of the InP island geometry. Both theoretical PL curves are based on full 3D simulations, including the piezoelectric potential. However, the solid blue/gray line was computed with InP islands having the shape of a truncated cone (axisymmetric), whereas the dashed line correspond to simulations based on the InP island geometry of Fig. 1. Figure 5(b) shows the effect of the piezoelectric potential in the case of an axisymmetric InP island. The numerical PL curves have been normalized by equating their QD4 peak to the corresponding QD4 peak of the experiments.

of the transition energies $E_{\hbar\omega}=E_i-E_f$, due to the size distribution of the SIQDs, was approximated using the Gaussian broadening function $P(E,\Gamma)$,[20,21] where Γ is the inhomogeneous linewidth. The Lorentz shaped homogeneous linewidth broadening (due to the finite life times of the QD eigenstates) was neglected, because it has a vanishing effect on the PL, which is also inhomogeneously broadened. In the calculations of Fig. 5 we have assumed complete state filling, i.e., the Fermi functions of electrons and holes were $f_e(E_i)=1$ and $f_h(E_f)=1$, respectively. On the basis of the experimentally observed size distribution of InP stressor islands[22] we have estimated $\Gamma=6$ meV.

Figure 5 shows the simulated PL spectrum, averaged over the polarization, for an ensemble of SIQDs together with an experimental luminescence spectrum. Figure 5 shows also the effect of the exact InP island geometry and of the PEP on the PL spectrum. All results are based on fully three-dimensional simulations. However, in the axisymmetric model we used an InP island having the shape of a truncated cone with the same height, the same InP volume and the same bottom area as the angular island, shown in Fig. 1(b). We note that the PEP affects mainly the PL peaks corresponding to transitions between excited states (QD3, QD4, QD5), whereas the angular island geometry (the deviation from the axisymmetry) increases the peak-peak energy separation and sharpens the peak profiles.

The calculation of radiative transition energies and line strengths shows good agreement with the experimental intensity distribution and energy spacing of the luminescence

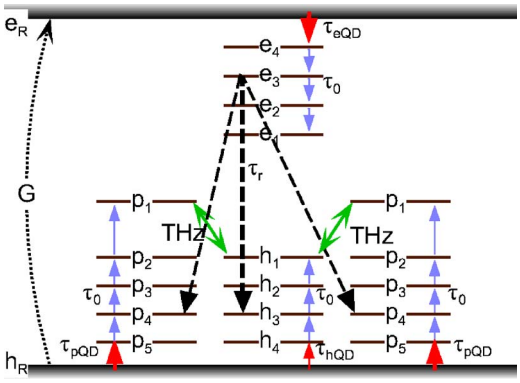

FIG. 6. (Color online) Carrier dynamics model. The eigenstates of the DP minima are labeled e_i and h_i; the hole states of the PEP minima are labeled p_i. The pump laser G generates carriers to the reservoirs (e_R and h_R) and the resonant THz radiation transfers holes between the ground states p_1 and h_1. Radiative recombinations (black dashed arrows) are shown for the third electron level only. The energy scale is only schematic.

peaks.[7] Each peak consists of many different transitions which after the convolution of inhomogeneous broadening form a smooth and continuous spectrum, well reproducing the experimental PL. A characterization of the PL peaks, according to the symmetry of the involved eigenstates, is difficult due to the weak confinement and small energy spacing (1–4 meV) of hole states. Only the two lowest peaks (QD1 and QD2) are due to recombination between clearly confined electron and hole states. The higher PL peaks are due to recombination between a few confined electron states and several confined or quasiconfined hole states (i.e., the hole states are shared between the DP and PEP minima, with their energies merging with the energy continuum of the QW).

III. DYNAMICAL MODEL

The presence of the PEP minima makes the relaxation pathways decisively different from conventional QD carrier dynamics, especially for holes, for which the piezoelectric side barriers (shown in Fig. 2) block the relaxation to the DP minimum along the y axis. The relaxation of holes along the x axis to the DP minimum is hindered as well, but by the PEP minima which capture the holes before they can enter the DP minima. The inefficient hole relaxation was also observed in the experiments as weak QD luminescence during Ti-Sap carrier generation directly to the QW. This indicated a very inefficient carrier relaxation from the QW to the radiative states of the SIQDs unless the carriers of the QW were *hot*, as in the case of Ar-ion laser pumping.

On the basis of these observations we have developed the carrier dynamics model, schematically shown in Fig. 6. This model is a generalization, based on a true three-dimensional description of the QD system, of the models presented in Refs. 9 and 5, which are as such not able to describe the experiments analyzed here.

A. Underlying assumptions

Our carrier dynamics model is based on the following assumptions, which are motivated by both experimental observations and theoretical studies.

(i) *The carrier population is charge neutral.* This implies that the total number of holes (including the valence states of the DP minimum, the two PEP minima and the QW) is equal to the total number of electrons (including the conduction states of the DP minimum and the QW). This is motivated for undoped samples were the optical carrier generation and recombination conserves the net charge, except for small charge fluctuations between different QDs, which mainly broaden the PL peaks. The assumption of charge neutrality is also supported by the invariance of the experimentally measured line energies in SIQD luminescence spectra, as a function of state filling; i.e., the luminescence energies are independent on the filling of eigenstates.[7,23] If there was a change in the net charge, there would also be a noticeable change in the line energies.

(ii) *The total number of electron and hole states, included in the model, were equal.* The number of electron and hole states was limited to $N \sim 100$, in order to stabilize the MC simulations and to account for the possible saturation of carrier generation to the QW reservoirs. This was done by setting the total number of electron states equal to the total number of hole states of the entire model. This has little effect on the QD luminescence character as we are typically far from saturation, but this is in accordance with assumption (i).

(iii) *We excluded the possibility of nonradiative recombination channels.* Nonradiative recombinations are typically a result of crystal imperfections or interface states and they are indirectly observed in terms of very short luminescence lifetimes. The self-organized samples of SIQDs are of very high quality, showing very long luminescence life times of ~ 1 ns.[5] The nonradiative recombination channels are thus rare.

(iv) *Nearly degenerate electron and hole states were combined to a few degenerate levels.* The DOS had to be simplified in order to make the MC calculations numerically feasible. The original DOS contained too many states to be included in the MC model. However, the simplified DOS resembles well the true multiband three-dimensional DOS.

(v) *We accounted for the spin of the carriers.* The preservation of the spin quantum number influences the total speed of recombination. The conservation of the spin should be accounted for in any carrier dynamics model, however, it has to our knowledge not been accounted for in previous QD relaxation models. Note, that the spin is in general not a good quantum number for states of the eight-band effective-mass Hamiltonian, since the valence bands are strongly coupled by the spin-orbit interaction. In the present case, the spin is, however, an approximately good quantum number for both electron and hole states. This is due to the vertical confinement and biaxial strain of the QW, which cause the most strongly confined hole states to be nearly pure heavy-hole states, which have a well defined spin.

(vi) *The intraband relaxation time τ_0 was assumed ten times smaller than the radiative life times*. An equal intraband relaxation time of both electrons and holes is motivated for high carrier densities in which the carrier relaxation is dominated by Coulomb scattering and the Auger process.[5,6] From experiments[5,6] we know that at relatively high state filling the intraband relaxation is one order of magnitude faster than the radiative recombination. Furthermore, we assumed that relaxation takes place between consecutive states only.

(vii) *The tunneling rate between the PEP and DP minima was assumed zero.* This tunneling rate is small in comparison with the prevailing relaxation and recombination rates, since the spatial separation of the DP and PEP minima is about 20–30 nm.

(viii) *It was assumed that an intense THz radiation can couple the hole states p_1 and h_1.* If the intensity of the THz radiation is large and if the THz photon energy matches the energy separation of h_1 and p_1 it gives rise to a resonant charge transfer where the absorption (hole: $p_1 \rightarrow h_1$) and emission (hole: $h_1 \rightarrow p_1$) of THz photons compete. The radiation field is assumed to be in resonance with the h_1 DP state and *any* of the deep PEP states, which are in the model described by a single degenerate level p_1. We neglect spontaneous emission, which is presumably small at high THz intensities. The strength of the hole transfer is, in the experiment, not limited to a very narrow THz frequency range since in the real SIQD sample the single resonance frequency of the model is replaced by a quasicontinuum of transition frequencies. The inhomogeneous size distribution of the QDs is likely to further broaden the otherwise narrow peaks of allowed THz-radiation frequencies of effective coupling.

The coupling strength between the PEP states p_1 and the DP states h_1 depends on the intensity of the THz field, the carrier populations of the involved hole levels and a phenomenological coupling constant. This coupling strength is the only free scaling constant in our model. The available experimental and numerical tools are currently far from enabling quantitative measurements or *ab initio* type calculations of this coupling constant. As a summarizing note on our relaxation model we recall that all model parameters, except the phenomenological THz-radiation coupling, are based on direct measurements (τ_{ri}, τ_0), fitting to experimental data (f_i), or electron structure calculations (g_i).[5–7]

B. Master equations

The time evolution of the electron (n_i^e) and hole (n_i^h) populations of the intermediate DP states are described by the following master equations for $2 \leq i \leq 4$:

$$\frac{dn_i^e}{dt} = \frac{n_{i+1}^e(g_i - n_i^e)}{\tau_0} - \frac{n_i^e(g_{i-1} - n_{i-1}^e)}{\tau_0} - \frac{n_i^e n_i^h}{g_i \tau_{ri}} f_i - \frac{n_i^e[n_{(i+1)A}^p + n_{(i+1)B}^p]}{2g_i \tau_{ri}}(1 - f_i), \tag{3}$$

$$\frac{dn_i^h}{dt} = \frac{n_{i+1}^h(g_i - n_i^h)}{\tau_0} - \frac{n_i^h(g_{i-1} - n_{i-1}^h)}{\tau_0} - \frac{n_i^e n_i^h}{g_i \tau_{ri}} f_i, \tag{4}$$

and for the PEP states with $2 \leq i \leq 5$

$$\frac{dn_i^p}{dt} = \frac{n_{i+1}^p(g_i^p - n_i^p)}{\tau_0} - \frac{n_i^p(g_{i-1}^p - n_{i-1}^p)}{\tau_0} - \frac{n_{i-1}^e n_i^p}{2g_i\tau_{ri}}(1-f_{i-1}). \tag{5}$$

The time evolution of the ground state ($i=1$) populations are given by

$$\frac{dn_1^e}{dt} = \frac{n_2^e(g_1 - n_1^e)}{\tau_0} - \frac{n_1^e n_1^h}{g_1\tau_{r1}}f_1 - \frac{n_1^e[n_{2A}^p + n_{2B}^p]}{2g_1\tau_{r1}}(1-f_1), \tag{6}$$

$$\frac{dn_1^h}{dt} = \frac{n_2^h(g_1 - n_1^h)}{\tau_0} - \frac{n_1^e n_1^h}{g_{r1}\tau_{r1}}f_1 + [g_1(n_{1A}^p + n_{1B}^p) - 2n_1^h g_1^p]G_{\mathrm{THz}}, \tag{7}$$

$$\frac{dn_{1\gamma}^p}{dt} = \frac{n_{2\gamma}^p(g_1^p - n_{1\gamma}^p)}{\tau_0} + (n_1^h g_1^p - n_{1\gamma}^p g_1^p)G_{\mathrm{THz}}, \tag{8}$$

and for the reservoirs ($i=R$) we have

$$\frac{dn_R^e}{dt} = -\frac{n_R^e(g_4 - n_4^e)}{\tau_{eQD}} - \frac{n_R^e n_R^h}{g_R\tau_R} + G, \tag{9}$$

$$\frac{dn_R^h}{dt} = -\frac{n_R^h(g_4 - n_4^h)}{\tau_{hQD}} - \frac{n_R^h(2g_5^p - n_{5A}^p - n_{5B}^p)}{\tau_{pQD}} - \frac{n_R^e n_R^h}{g_R\tau_R} + G, \tag{10}$$

where the two PEP minima are identified by subindices $\gamma = iA$ and $\gamma = iB$. As explained below G_{THz}, in Eqs. (3)–(10), is the THz-radiation intensity and $G=(g_R^e - n_R^e)(g_R^h - n_R^h)G_{\mathrm{exc}}$ is the carrier generation rate by the pump laser G_{exc}. We also accounted for the spin of the carriers, which effectively raised the population of excited states. A detailed analysis of Eqs. (3)–(10) follows below.

C. Partial transition rates

The MC carrier dynamics model is depicted in Fig. 6 and was given in mathematical form in Eqs. (3)–(10). It describes the time evolution of the electron n_i^e and hole n_i^h populations of the DP states as well as the hole populations n_{iA}^p and n_{iB}^p of the PEP states (left and right minima).

1. The population of intermediate states

The time evolution of the electron and hole populations n_i^e and n_i^h of the intermediate states (i.e., $2 \le i \le 4$) of the DP minima are described by Eqs. (3) and (4). The population of state i is increased by the intraband relaxation (colored/gray arrows in Fig. 6) from state $i+1$ to state i [first term on the right hand side (RHS) of Eqs. (3) and (4)] and reduced by the carrier relaxation to state $i-1$ [second term on the RHS of Eqs. (3) and (4)]. The rate of the intraband relaxation is described by the intraband relaxation lifetime τ_0, which is typically one tenth of the radiative lifetime τ_r.[6]

The main recombination processes involve electron and holes (the center black dashed arrow in Fig. 6), both confined in the DP minima, and are described by the third term on the RHS of Eqs. (3) and (4). The recombination of electrons in the DP minimum and holes in the PEP minima is described by the fourth term on the RHS of Eq. (3) (left and right, black dashed arrows in Fig. 6). This rate is weaker than the recombination rate between the DP states, due to the small spatial overlap of the pertinent wave functions. The different transition probabilities of the DP→DP and DP→PEP recombination could be included by using different time constants. However, in our model it has been more convenient to describe this effect by the ratios $f_i/(1-f_i)$. The numerical values of f_i were determined by fitting the state filling (PL peak intensities), as a function of the generation rate, to experimental PL data.[7,23]

The time evolution of the hole populations n_i^p of the intermediate (i.e., $2 \le i \le 5$) states of the PEP minima are described by Eq. (5). The first and second terms on the RHS correspond to intraband relaxation (colored/gray arrows in Fig. 6) from state $i+1$ to state i and from state i to $i-1$, respectively. The last term corresponds to radiative recombination with electrons confined in the DP minimum (left and right, black dashed arrows in Fig. 6).

2. The population of the DP and PEP ground states

The time evolution of the electron ground state population n_1^e is described by Eq. (6), which is similar to Eq. (3), except that it does not contain the second term of the RHS of Eq. (3) as the holes cannot relaxate any further from the ground state. Equation (7) describes the time evolution of the hole population of the DP ground state. The first and second terms on the RHS correspond to intraband relaxation from state $i+1$ to state i (colored/gray arrows in Fig. 6) and to radiative recombination (center black dashed arrow in Fig. 6) between electron and holes of the DP minima. The third term correspond to the THz radiation-induced coupling of the states $h1$, $p1A$ (in the left PEP minimum) and $p1B$ (in the right PEP minimum). It accounts for the absorption of a THz photon, exciting a hole from state $h1$ to states $p1A$ or $p1B$, and the stimulated emission of a THz photon, taking a hole from state $p1A$ to $h1$ or from state $p1B$ to $h1$. These processes are indicated by double-headed arrows in Fig. 6.

The time evolution of population $n_{1\gamma}^p$ of the deepest PEP states is described by Eq. (8), where $\gamma=A$ or $\gamma=B$ correspond to left and right PEP minimum, respectively. The first term on the RHS corresponds to the intraband relaxation from state $p2$ to state $p1$ (colored/gray arrows in Fig. 6). The second term accounts for both the emission or absorption of a THz photon (simultaneously moving a hole from state $p1\gamma$ to state $h1$).

3. The population of the reservoirs

The QW, embedding the SIQDs is modeled as a reservoir of electrons and holes, with the state degeneracies g_R^e and g_R^h, both being much larger than the degeneracies of the QD levels. The electron and hole reservoirs are described by Eqs. (9) and (10), respectively. The first term on the RHS of Eq. (9) [Eq. (10)] describes the capturing of an electron (hole) from the reservoirs to the DP minimum with the capture lifetime τ_{eQD} (τ_{hQD}) describing the rate of this process. The second term on the RHS of Eq. (9) and the third term on the

RHS of Eq. (10) account for the radiative recombination of electrons and holes in the reservoirs, with the corresponding lifetime τ_R. The second term of Eq. (10) is due to holes getting captured into the two (A and B) PEP minima. The carrier generation is described by the last term of both Eq. (9) and (10).

D. General remarks on the model parametrization

We note that the radiative lifetimes of SIQDs have been measured and modeled successfully previously.[5,6] In our carrier dynamics model we used radiative lifetimes τ_{ri} ($\tau_{ri} > \tau_{rj} \approx 10\tau_0$, for all $i > j$), which were calculated from the eight-band electron structure model in the electric dipole approximation and were in good agreement with experiments. The radiative recombination rates of the $p1$ states were found negligible. We found that the radiative recombination rates of also the lower excited PEP states (pi, with $i \lesssim 4$) were noticeable longer than those of the corresponding DP states. We used, therefore, recombination lifetimes $\tau'_{ri} = \tau_{ri}/(1-f_i)$ with $0 < f_i < 1$ for the excited states of the PEP minima. The exact values of f_i were determined by fitting the state filling (PL peak intensities) to experimental data.[23] The distinction between DP and PEP states becomes, however, difficult for highly excited states, since these states are not confined in only one minimum, but the probability densities are shared between all three minima.

The intraband relaxation time constant τ_0 affects, together with the amplitudes of the individual recombination processes, the relative CW intensities and the rates of fading off of the PL peaks. The effect of the THz radiation on the QD PL is not very sensitive to τ_0 at low generation intensities. However, the smaller τ_0 is, the smaller generation intensity is needed to saturate the hole population of $h1$ (even without any THz radiation). The value of τ_0 does thereby affect the threshold value of the generation intensity at which the THz-radiation-induced PL effect disappears.

The validity of the used radiative and intraband relaxation time constants, describing the carrier dynamics in the absence of any THz radiation, was verified by comparing the numerical time dependent PL of our model with experiments. On the basis of this comparison we conclude that our model is very well in line with Refs. 23 and 5 (see also Fig. 5).

Equations (3)–(10) were solved by time-dependent MC simulations[24] of a large ensemble of independent QDs. We obtained the probabilities of each many-particle partition as a function of time by averaging over the ensemble populations. By simulating QD ensembles large enough (a few thousands of QDs) we were able to minimize the time-dependent oscillations of simulated quasistationary partitions during steady state laser modulation.

IV. DISCUSSION AND CONCLUSIONS

A. Luminescence during continuous pumping

The free carriers can relax from the GaAs barrier to the DP and PEP minima, either directly or through the QW state continuum. The direct relaxation is assisted by the funnel shaped deformation and piezoelectric potential minima in the barriers.[11] As the holes are predominantly confined in the deep PEP minima, the radiative recombination starts only when these minima are already filled with holes. A saturated QD is consequently strongly polarized during continuous generation and recombination. The charge separation, with holes in the PEP minima and electrons in the DP minimum, can persist even seconds after turning off the carrier generation.

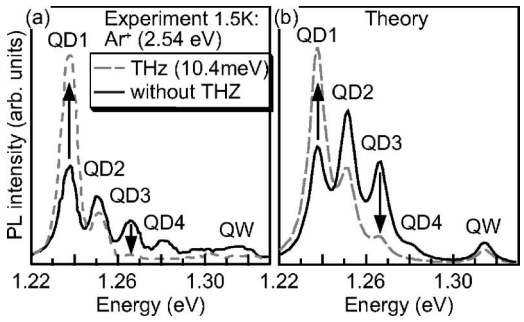

FIG. 7. Experimental (a) and theoretical (b) photoluminescence from a sample pumped by an Ar^+ laser only (solid lines) and by Ar^+ laser and FEL simultaneously (dashed line). The FEL energy of the experiments was $\hbar\omega_{THz} = 10.4$ meV.

The picture described above does not account for any excitonic carrier-carrier interactions. Previous studies have, however, shown that the carrier-carrier correlation effects are small in SIQDs.[25] The very good qualitative agreement between the experimental CW PL and the PL simulated here does also support the used single-particle approximation. The exciton effects of SIQDs are, though, fairly vaguely understood and do call for further studies.

B. Influence of THz radiation on the steady-state luminescence

According to our simulations, the enhancement of the QD1 luminescence is due to a THz-radiation-induced continuous drift of holes between the PEP p_1 levels and the DP h_1 level (Fig. 8). Under steady-state condition the total integrated PL intensity is conserved in the first approximation. The QD2, QD3, QD4, and QW peaks are accordingly reduced when the QD1 peak is increased by the THz radiation, both in the experiment and theory. Our calculations predict furthermore that the THz-radiation enhancement of the QD1 peak disappears at high Ar^+ pumping intensities as a result of the saturation of the hole population at h_1.

The results are in good qualitative agreement with the experiments, although, a quantitative agreement cannot be achieved with the current model. Our model does not show as dramatic quenching of the QW PL by the THz radiation as was seen in the experiment, although, Figs. 7 and 8 do show a clear decrease of the QW PL. We argue that the large decrease of the experimental QW PL is related to the heating and ionization of QW excitons.[26]

The discrepancies between the intensity distributions of the PL peaks (in Fig. 7) of our model and of the experiments are mainly due to the simplified electronic structure used in our MC model and the fact that we have used the same relaxation life time for all hole and electron states. A better

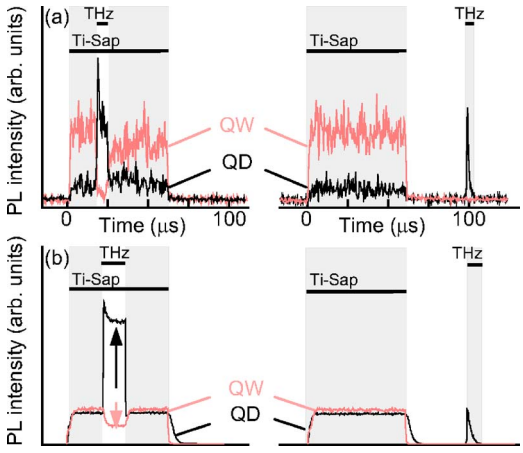

FIG. 8. (Color online) Experimental (a) and simulated (b) time-resolved PL of the QD ground state (black) and QW (red) for $T=15$ K. The energy and power of the THz radiation were $\hbar\omega_{\mathrm{THz}}=2.5$ meV and $P=1$ kW, respectively. The time windows of the Ti-Sap laser (carrier generation to the QW) and THz-radiation are indicated by horizontal bars.

fit between the simulations and experiments could have been obtained by using, e.g., several different relaxation rates between the different hole levels. This would, however, have made the model less transparent. The exact PL intensity distribution between the different peaks is also very much dependent on the carrier generation rate. This is true for both the simulations and the experiments (see, e.g., Ref. 9). Figure 4 was plotted for a carrier generation rate where the simulated QD2 peak already exceeds the QD1 peak. This generation rate was chosen, in order to obtain as clear THz effect as possible.

C. THz-radiation-induced transients

Figures 8(a) and 8(b) show experimental and simulated time-resolved PL. The black and red curves correspond to integrated PL of the QD1 and QW peaks, respectively. The left panels show results obtained for overlapping time windows of Ti-Sap pumping and THz-radiation excitation. The QW peak is decreased and the QD1 PL is increased during the THz radiation with both PL peaks returning to their initial value after turning off the THz radiation. Note the saturation of both the experimental and theoretical PL during THz radiation.

D. THz-radiation-induced delayed PL

The right panels of Fig. 8 show PL with a delayed THz-radiation pulse after turning off the pump laser. The rise of the QD1 peak by the delayed THz-radiation is due to the excitation and drift of trapped holes from the PEP minima to the DP minimum, where they recombine with electrons localized in the DP minimum. The simulation time was much smaller than that of the experimental time scale, due to computational limitations. However, the time scale of the simulations were chosen long enough to observe saturation of the PL both during the pumping and between the pumping and the delayed THz radiation. There is also in this case a very good qualitative agreement between experiments and theory.

V. CONCLUSION

We have shown that the anomalous cooling of radiative QD excitons[4] is due to a THz-radiation-induced drift of holes from piezoelectric potential (PEP) minima to the lowest radiative states of the QD. The subsystem of radiative excitons is cooled, although, the average energy of the total carrier system increases (heated).

By cooling of the radiative exciton subsystem we mean that the average hole population of the ground state $h1$ increases whereas the average population of all excited states in the deformation potential (DP) minimum decreases. The large shift of the particle population (within the radiative states) from the excited states towards the ground state is analogous to lowering of the temperature in a system of thermal equilibrium. However, the carriers of our SIQDs are not in thermal equilibrium nor in thermal quasiequilibrium during continuous (or transient) carrier generation and THz modulation. Therefore, the reduction of the average energy of the radiative excitons cannot be called lowering of the carrier temperature.

Our computational model reproduces currently the following experimental observations on SIQDs. (i) The simulated CW PL reproduces experimental data[23] as a function of the carrier generation intensity. (ii) The THz radiation increases the ground state luminescence and decreases the excited state luminescence at low generation intensities during CW THz excitation. (iii) At the onset of the THz radiation there is a strong and sudden increase of the QD1 luminescence. The enhancement by the THz radiation is then, however, exponentially reduced and saturates at a lower level. (iv) The THz radiation gives rise to ground state luminescence long after turning off the carrier generation. This delayed PL flash is seen only in the ground state luminescence and it fades out exponentially.

The ultimate goal of our work is to motivate new experiments in which the THz-photon energy would be varied over a wide energy range, covering several *pi* and *hi* levels. We argue that the analysis of the original experiments by Yusa *et al.* is necessary for a careful planning of further experiments. Finally, we note that our simulations suggest that the resonance transfer by THz radiation could be replaced by a bias voltage-driven resonance tunneling, leading to an enhanced QD ground state luminescence.

ACKNOWLEDGMENTS

We gratefully acknowledge the fruitful communications with Harri Lipsanen and the computational effort by Roman Terechonkov on the electronic structure calculations.

*Electronic address: fredrik.boxberg@tkk.fi

[1] M. A. Kastner, Phys. Today **46**, 24 (1993).
[2] P. Michler, A. Kiraz, C. Becher, W. V. Schoenfeld, P. M. Petroff, Lidong Zhang, E. Hu, and A. Imamoglu, Science **290**, 2282 (2000).
[3] J. P. Reithmaier, G. Sek, A. Löffler, C. Hofmann, S. Kuhn, S. Reitzenstein, L. V. Keldysh, V. D. Kulakovskii, T. L. Reinecke, and A. Forchel, Nature (London) **432**, 197 (2004).
[4] G. Yusa, S. J. Allen, J. Davies, H. Sakaki, H. Kono, J. Ahopelto, H. Lipsanen, M. Sopanen, and J. Tulkki, Proceedings of the 24th ICPS, *Teraherz-Near Infrared Upconversion in Strain-Induced Quantum Dots*, (World Scientific, Singapore, 1999).
[5] S. Grosse, J. H. H. Sandmann, G. von Plessen, J. Feldmann, H. Lipsanen, M. Sopanen, J. Tulkki, and J. Ahopelto, Phys. Rev. B **55**, 4473 (1998).
[6] M. Braskén, M. Lindberg, M. Sopanen, H. Lipsanen, and J. Tulkki, Phys. Rev. B **58**, R15993 (1998).
[7] H. Lipsanen, M. Sopanen, and J. Ahopelto, Phys. Rev. B **51**, 13868 (1995).
[8] D. M. Wood and Alex Zunger, Phys. Rev. B **53**, 7949 (1996).
[9] M. Grundmann and D. Bimberg, Phys. Rev. B **55**, 9740 (1997).
[10] A. J. Williamson, L. W. Wang, and Alex Zunger, Phys. Rev. B **62**, 12963 (2000).
[11] J. Tulkki and A. Heinämäki, Phys. Rev. B **52**, 8239 (1995).
[12] K. Georgsson, N. Carlsson, L. Samuelson, W. Seifert, and L. R. Wallenberg, Appl. Phys. Lett. **67**, 2981 (1995). The InP stressors of this work were similar to those of the presently studied sample, however, these samples did not contain any QW.
[13] S. v Alfthan, F. Boxberg, K. Kaski, A. Kuronen, R. Tereshonkov, J. Tulkki, and H. Sakaki, Phys. Rev. B **72**, 045329 (2005).
[14] All elasticity calculations were performed using the commercial software ANSYS.
[15] R. Virkkala, K. Maijala, and J. Tulkki, Phys. Rev. B **62**, 6932 (2000). The results reported in the current article differ from the earlier ones due to a decisively improved electroelastic model and more rigorous accounting of the crystal and island symmetry.
[16] Craig Pryor, Phys. Rev. B **57**, 7190 (1998).
[17] O. Stier, *Electronic and Optical Properties of Quantum Dots and Wires* (Wissenschaft und Technik Verlag, Berlin, 2001).
[18] H. Jiang and J. Singh, IEEE J. Quantum Electron. **34**, 1188 (1998).
[19] Society for Industrial and Applied Mathematics, ARPACK *Users' Guide: Solution of Large-Scale Eigenvalue Problems with Implicitly Restarted Arnoldi Methods*, 1998.
[20] Marius Grundmann and Dieter Bimberg, Jpn. J. Appl. Phys., Part 1 **36**, 4181 (1997).
[21] Omar Qasaimeh, IEEE Trans. Electron Devices **50**, 1575 (2003).
[22] *Optics of Quantum Dots and Wires*, edited by Garnett W. Bryant and Glenn S. Solomon (Artech House, Boston, 2005).
[23] H. Lipsanen, M. Sopanen, and J. Ahopelto, Solid-State Electron. **40**, 601 (1996).
[24] C. Wasshuber, *Computational Single-Electronics* (Springer, Wien, 2001), Chap. 3.
[25] M. Braskén, M. Lindberg, D. Sundholm, and J. Olsen, Phys. Rev. B **64**, 035312 (2001).
[26] J. Cerne, J. Kono, M. S. Sherwin, M. Sundaram, A. C. Gossard, and G. E. W. Bauer, Phys. Rev. Lett. **77**, 1131 (1996).
[27] *Numerical data and functional relationships in science and technology*. Landolt-Börnstein. New Series, III/17a (Springer, Berlin, 1991).
[28] J. Singh, *Physics of Semiconductors and Their Heterostructures* (McGraw-Hill, New York, 1993).
[29] I. Vurgaftman, J. R. Meyer, and L. R. Ram-Mohan, J. Appl. Phys. **89**, 5815 (2001).